CO_2 Hydrate: Synthesis, Composition, Structure, Dissociation Behavior, and a Comparison to Structure I CH_4 Hydrate

Susan Circone,*,† Laura A. Stern,† Stephen H. Kirby,† William B. Durham,‡ Bryan C. Chakoumakos,§ Claudia J. Rawn,§ Adam J. Rondinone,§ and Yoshinobu Ishii⊥

U.S. Geological Survey, 345 Middlefield Road, MS 977, Menlo Park, California 94025, Lawrence Livermore National Laboratory, Livermore, California 94550, Oak Ridge National Laboratory, Oak Ridge, Tennessee 37831, and Japan Atomic Energy Research Institute, Tokai, Ibaraki, Japan

Received: November 5, 2002; In Final Form: February 25, 2003

Structure I (sI) carbon dioxide (CO_2) hydrate exhibits markedly different dissociation behavior from sI methane (CH_4) hydrate in experiments in which equilibrated samples at 0.1 MPa are heated isobarically at 13 K/h from 210 K through the H_2O melting point (273.15 K). The CO_2 hydrate samples release only about 3% of their gas content up to temperatures of 240 K, which is 22 K above the hydrate phase boundary. Up to 20% is released by 270 K, and the remaining CO_2 is released at 271.0 ± 0.5 K, where the sample temperature is buffered until hydrate dissociation ceases. This reproducible buffering temperature for the dissociation reaction $CO_2 \cdot nH_2O = CO_2(g) + nH_2O(l \text{ to } s)$ is measurably distinct from the pure H_2O melting point at 273.15 K, which is reached as gas evolution ceases. In contrast, when sI CH_4 hydrate is heated at the same rate at 0.1 MPa, >95% of the gas is released within 25 K of the equilibrium temperature (193 K at 0.1 MPa). In conjunction with the dissociation study, a method for efficient and reproducible synthesis of pure polycrystalline CO_2 hydrate with suitable characteristics for material properties testing was developed, and the material was characterized. CO_2 hydrate was synthesized from CO_2 liquid and H_2O solid and liquid reactants at pressures between 5 and 25 MPa and temperatures between 250 and 281 K. Scanning electron microscopy (SEM) examination indicates that the samples consist of dense crystalline hydrate and 50−300 μm diameter pores that are lined with euhedral cubic hydrate crystals. Deuterated hydrate samples made by this same procedure were analyzed by neutron diffraction at temperatures between 4 and 215 K; results confirm that complete conversion of water to hydrate has occurred and that the measured unit cell parameter and thermal expansion are consistent with previously reported values. On the basis of measured weight gain after synthesis and gas yields from the dissociation experiments, approximately all cages in the hydrate structure are filled such that $n \approx 5.75$.

Introduction

Carbon dioxide hydrate, $CO_2 \cdot nH_2O$ ($n \geq 5.75$), belongs to a family of nonstoichiometric compounds in which hydrogen-bonded water molecules are arranged in an icelike framework, forming polyhedral cavities occupied by "guest" molecules with an appropriate size range. CO_2 hydrate crystallizes in one of the two cubic hydrate structures (structure I), in which the unit cell consists of 46 H_2O (or D_2O) molecules and up to 8 CO_2 molecules occupying both small (pentagonal dodecahedral) and large (tetrakaidecahedral) cavities in a ratio of 1:3. CO_2 hydrate is stable over a range of elevated pressure and low-temperature conditions (see Sloan[1] for a summary of the published phase equilibria data). The formation of CO_2 hydrate from H_2O ice has been observed optically,[2,3] and synthetic CO_2 hydrate has been studied by a number of techniques, including NMR spectroscopy,[4,5] IR spectroscopy,[6] X-ray diffraction,[7,8] and neutron diffraction.[9−11] These studies indicate that CO_2 occupies both cavities in the sI hydrate structure, having approximately full occupancy of the larger cavities and variable occupancy of the small cavities, dependent on the synthesis conditions. In naturally occurring gas hydrates, CH_4 typically is the principal "guest" molecule with a variety of condensed alkanes and inorganic gases such as N_2, H_2S, and CO_2 present as additional constituents.

Concerns about the effect of greenhouse gases, such as atmospheric CO_2 produced by fossil fuel combustion, on global warming have intensified in the past decade. Sequestering large amounts of liquid CO_2 in deep ocean settings has been proposed. Numerous researchers have observed the interaction between CO_2 liquid and seawater in the laboratory (e.g., ref 12) and in a natural setting, where researchers observed the direct release of gaseous and liquid CO_2 at a range of depths in the ocean.[13] Investigations of CO_2 hydrate properties and reaction kinetics, in the laboratory as well as in marine settings, are relevant to the possible large-scale disposal of liquid CO_2 in deep ocean environments, where CO_2 hydrate readily forms at the CO_2 liquid−seawater interface. With this purpose in mind, we have built on preliminary work in the CO_2−H_2O system[2,3] to (1) find a reliable, reproducible, and efficient method for CO_2 hydrate synthesis, (2) characterize the texture, structure, and composition of this material, (3) investigate the dissociation behavior of CO_2 hydrate in a CO_2 gas atmosphere at 0.1 MPa, including comparison with sI CH_4 hydrate studied under similar condi-

* To whom correspondence should be addressed. Phone: 650/329-5674. Fax: 650/329-5163. E-mail: scircone@usgs.gov.
† U.S. Geological Survey.
‡ Lawrence Livermore National Laboratory.
§ Oak Ridge National Laboratory.
⊥ Japan Atomic Energy Research Institute.

10.1021/jp027391j CCC: $25.00
Published on Web 00/00/0000 PAGE EST: 10.9

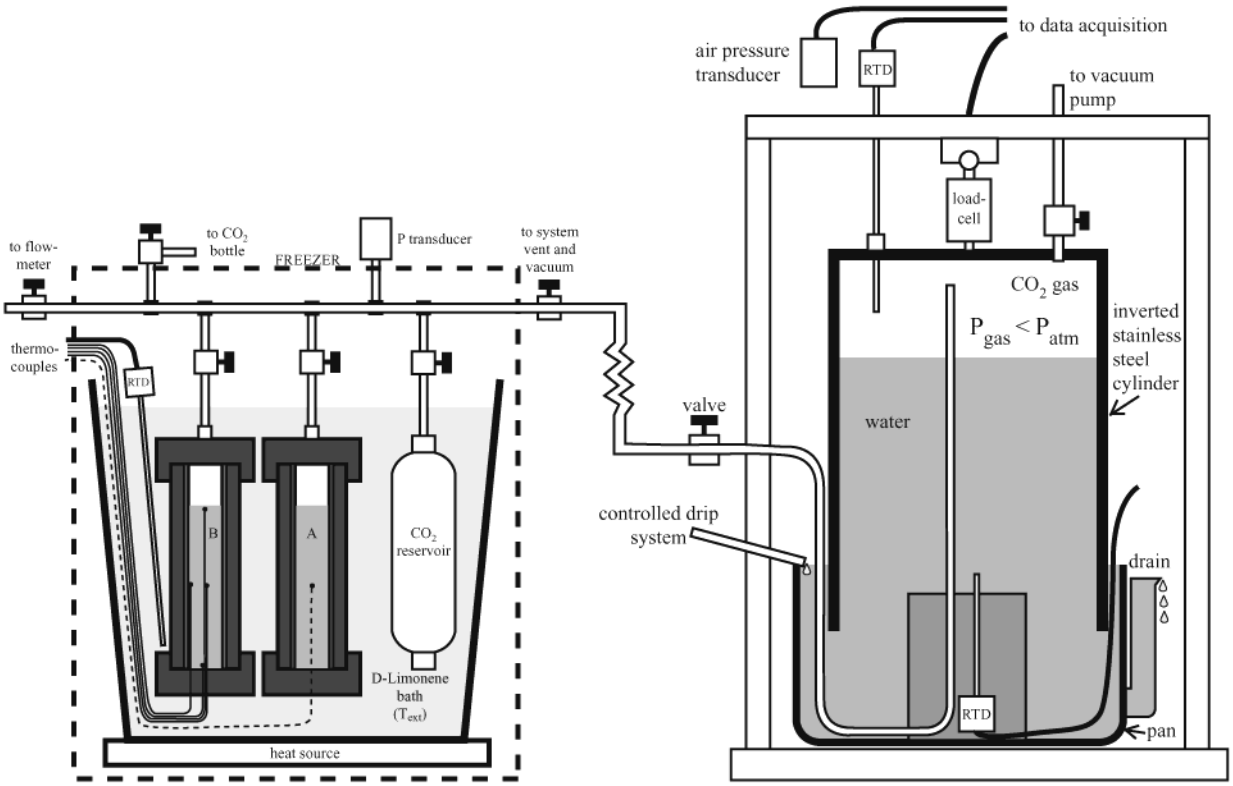

Figure 1. Schematic drawing (not to scale) of the synthesis apparatus showing the pressure vessels with internal thermocouple configurations, the CO_2 reservoir (150 cm^3), and their immersion in a bath of D-limonene. The apparatus is located in a commercial freezer, and the bath is heated from below to raise the temperature above the ambient freezer temperature (about 252 ± 3 K). Bath temperature (T_{ext}) is monitored with a resistance temperature detector (RTD). When an internal thermocouple is used in Sample A, it is located along the cylinder axis at the sample middle (height is 4.7 cm). In Sample B, three thermocouples are located along the cylinder axis at the top (8.9 cm from sample bottom), middle (4.7 cm), and bottom (0.6 cm) of the sample. A side thermocouple (4.8 cm) measures temperature a few millimeters in from the sample surface. The vessel interior is packed with granular H_2O(s) (shown as the gray-shaded space), and the free space is filled with CO_2 liquid (metal disks, not shown, are placed on the sample top to decrease the fluid volume). The thermocouples, RTD, and pressure transducer are interfaced with a data acquisition system. The apparatus is connected to a flow meter (modified from Figure 1 in Circone et al.[20]), which monitors CO_2 evolution during hydrate dissociation. As gas is released during hydrate dissociation, it is collected in the inverted, close-ended cylinder of the flow meter, which is suspended from a load cell. The evolved gas displaces the water in the column, and the corresponding weight change is measured over time and converted into moles of gas, from which the amount and rate of gas release is calculated. Refer to Circone et al.[20] for further details. The flow meter and controlled drip system are enclosed in CO_2 gas-filled bags (not shown) to keep the system saturated in CO_2.

tions,[14] and (4) provide well-characterized samples for a collaborative research project to determine the dissolution rates of CH_4 and CO_2 hydrates in a deep ocean setting.[15]

Experimental Methods

Synthesis Setup. Structure I CO_2 hydrate was synthesized starting from liquid CO_2 and solid H_2O using the methodology for synthesizing pure CH_4 hydrate[16] and also following a two-stage synthesis process for CO_2 hydrate used by Henning et al.[11] The synthesis apparatus and seed ice preparation have been described previously.[16] We synthesize two 2.54 cm diameter by 12 cm long cylinders of CO_2 hydrate at a time (Figure 1). There are two pressure vessels: vessel A had either no thermocouples or one centered internal thermocouple, and vessel B had four internal thermocouples (Figure 1). The pressure vessels were first packed at temperatures near 250 K with ~26 g of H_2O seed ice with a grain size of 180−250 μm and a nominal intergranular porosity of 52%. Deuterated samples were made from 29 g of D_2O seed ice and the same size fraction packed to a nominal intergranular porosity of 56%. The vessels are then suspended in a fluid bath housed in a conventional freezer. After evacuating the vessels for 1.5 min to remove air, they were first filled with cold CO_2 gas from the CO_2 reservoir and then slowly pressurized with room-temperature CO_2 liquid from a large bottle. Because the internal vessel temperature increased as warm CO_2 was introduced, the flow rate of CO_2 liquid was controlled to maintain the temperature below 260 K as the vessels were filled with CO_2 liquid to a pressure near 6 MPa, taking up to 0.5 h. The vessel interiors attained thermal equilibrium with the surrounding bath before we started the synthesis cycle, during which some hydrate formation occurred, as evidenced by a slow and steady decrease in CO_2 liquid pressure.

Synthesis Procedure. Initially, we synthesized CO_2 hydrate using a two-stage, two-cycle heating method. Samples were first heated to 267.5 K, 17 ± 2 MPa and held isothermal for approximately 20 h. Once all of the CO_2 gas in the system had condensed (by 255 K and 6.0 MPa), the pressure climbed rapidly during heating because of the low compressibility of the CO_2 liquid. Samples were then heated through the H_2O solidus to 280 ± 1 K, 23 ± 2 MPa and again held isothermal for approximately 20 h before cooling to ambient freezer temperatures near 250 K (cycle 1, Figure 2a). We checked for the presence of unreacted H_2O in the samples by looking for temperature or pressure increases during cooling through the H_2O ice point due, respectively, to heat release and to a volume increase upon H_2O freezing. This can be detected in samples containing a few percent unreacted H_2O, and these samples were heated again to 281 K, 20 ± 2 MPa and held isothermal for approximately 20 h before cooling to ambient freezer temper-

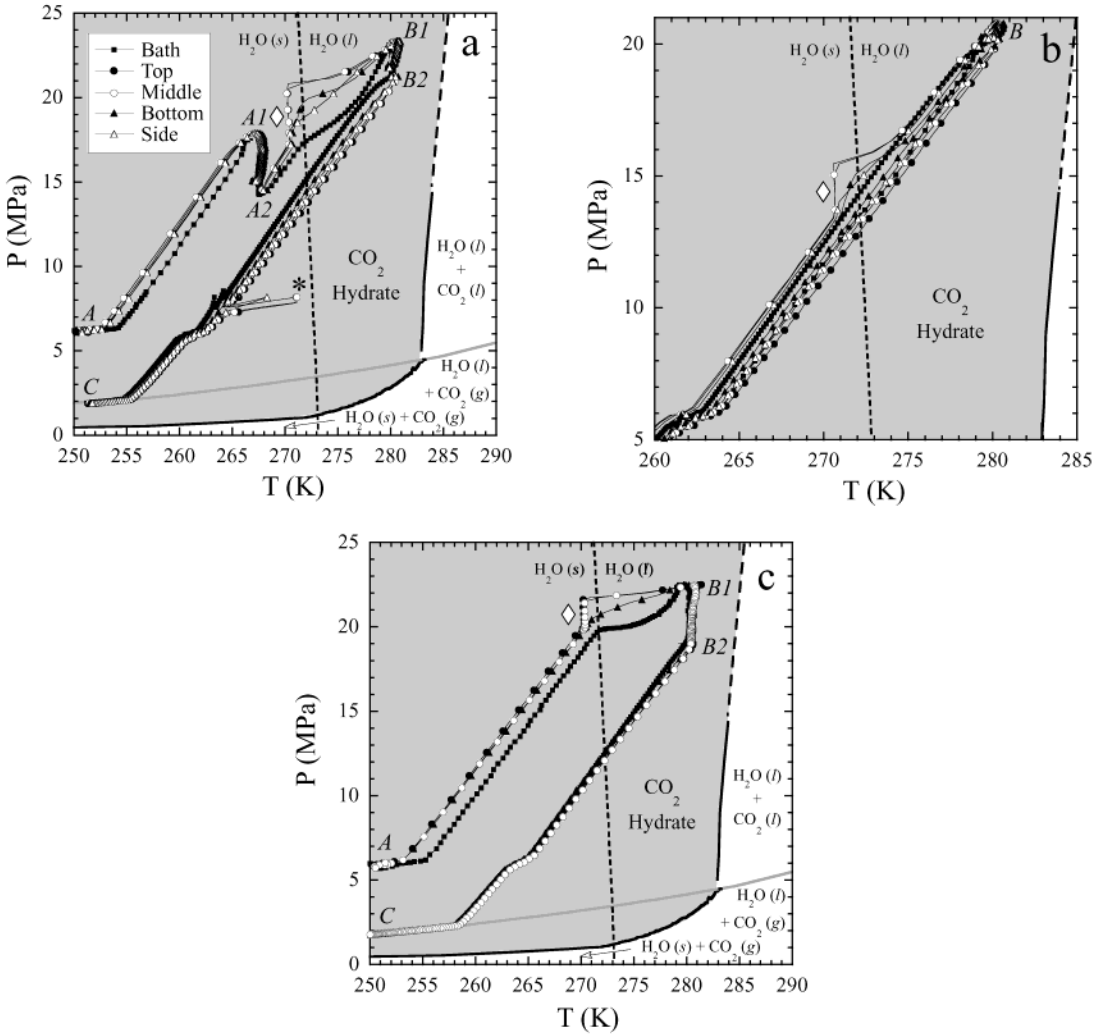

Figure 2. Pressure−temperature history during CO_2 hydrate synthesis by either a two-stage, two-cycle heating method (a, b) or a single-stage, one-cycle method (c). Phase boundaries for the CO_2−H_2O system (CO_2 hydrate = shaded area) and for the CO_2 gas/liquid boundary (gray line) are from the phase equilibria data summarized in Sloan;[1] the H_2O solid/liquid boundary is also shown (dashed line). Every fourth data point for internal sample temperatures is plotted, and all data for external bath temperature are plotted. In panel a, CO_2 pressure as a function of bath and sample temperatures is shown. Two-stage heating in the first cycle involves heating at a rate of 13 K/h to 267.5 K (A to A1) for a 20-hour isothermal hold (A1 to A2) and then heating to 281 K (A2 to B1) for a 20-hour isothermal hold (B1 to B2), followed by cooling back to ambient freezer temperature (B2 to C). The internal sample temperatures are displaced 1−2 K from the bath temperature (T_{ext}) during heating and cooling because of the delay in heat transfer through the pressure-vessel walls. This effect is more pronounced, especially during heating, in the sample interior (middle, top) than along the sample surfaces (bottom, side). The internal sample temperatures buffer near 270 K (◊) for up to 60 min and lag the external bath temperature by up to 8 K before eventually equilibrating with the bath. Note that data points at a given pressure are isotemporal such that at the diamond the temperature distribution in the bath and the sample interior were as follows: bath > side > bottom > top and middle of the samples. During cooling, the sharp CO_2 pressure increases near 264 K and 8 MPa coincide with the anomalous temperature increase (∗) observed in sample B (sample A did not contain internal thermocouples). The *P*, *T* slope flattens near 6 MPa during heating and cooling as the CO_2 gas condenses in the sections of tubing outside of the freezer (see Figure 1). By the end of cycle 1, the CO_2 pressure has dropped significantly because of hydrate formation, and the CO_2 liquidus is intersected near 256 K. Panel b shows CO_2 pressure as a function of bath and sample temperatures during cycle 2, which involves direct heating from near 250 to 281 K, followed by a 16 h isothermal hold at 281 K (B) before cooling to 250 K. The thermal lag near 270 K (◊) is again observed during heating; however, there is no anomalous pressure or temperature increase during cooling, and the pressure offset due to hydrate formation is greatly reduced in this cycle. Panel c shows CO_2 pressure as a function of bath temperature and internal sample temperatures during single-stage, single-cycle synthesis of CO_2 hydrate by direct heating to 281 K (A to B1), followed by a 50 h isothermal hold at 281 K (B1 to B2) before cooling (B2 to C). Again, a thermal lag near 270 K (◊) is observed, and upon cooling no anomalous increase in pressure or temperature is detectable. See text for a discussion of the significance of the thermal lags and anomalous changes in pressure and temperature.

ature (cycle 2, Figure 2b), at which point conversion of all H_2O to hydrate was complete. The two-stage heating process was used to make the deuterated sample analyzed by neutron diffraction (see below). In subsequent syntheses of CO_2 hydrate, a single heating stage from 252 to 282 K, followed by an isothermal hold for 30−50 h, resulted in complete conversion of the reactants to hydrate (Figure 2c). After synthesis, samples were either dissociated or recovered for further study (see below).

Sample Recovery. In earlier experiments in this laboratory, CO_2 hydrate was synthesized successfully both in bulk and microscopically in an optical cell apparatus using H_2O seed ice and CO_2 gas or liquid. The absence of pressure anomalies in the synthesis record of samples made at the highest pressures (up to 16 MPa) indicates that the conversion to hydrate was complete. However, recovered bulk samples were plagued by the presence of large amounts of solid CO_2 after quenching in liquid nitrogen, and further analysis of these samples using other

techniques (such as measuring the CO_2 content of the hydrate by weighing) was not possible.

More recently, we have been able to expel excess CO_2 by flushing with CH_4 gas. Henning et al.[11] were able to recover CO_2 hydrate samples free of excess CO_2 and without appreciable dissociation by flushing the samples with He. We tried flushing the samples with CH_4 because of a separate research interest in temporarily holding CH_4 and CO_2 hydrate samples together in the same vessel without partial dissociation or exchange.[15] Following synthesis, samples equilibrated near 252 K and 2.0 MPa (point C, Figure 2) such that CO_2 liquid filled the sample pore space. We released CO_2 from the system in several pulses over 1−1.5 h, until the pressure stabilized near 252 K at 1.0 MPa in the CO_2 gas-only phase field (Figure 2). Then samples were pressurized with CH_4 gas to 1.9 MPa and vented to 1.0 MPa, and this flushing cycle was repeated four to six times over the next 0.5 h to dilute the free CO_2. The sample vessels were isolated at pressure and removed from the synthesis apparatus, stored at 252 K and 1.0 MPa gas pressure for less than 0.5 h or for 48 h, and then plunged into liquid nitrogen while the gas pressure was dropped to 0.1 MPa. The CH_4 flushing did not remove all of the CO_2 gas but diluted it to the extent that, after depressurization to 0.1 MPa, no residual CO_2 solid was detected by powder X-ray diffraction or neutron diffraction analysis.

Some of the CH_4-flushed samples were dissociated and then analyzed by gas chromatography to determine whether there was any appreciable CO_2−CH_4 exchange. One sample, quenched in liquid N_2 within minutes after flushing, contained trace N_2 but no detectable CH_4. Another sample, stored for 48 h, showed the gas content to be nearly pure CO_2 with only 163 ppm of CH_4 and trace amounts of N_2. Given the very low levels of CH_4 incorporated in the gas released during hydrate dissociation, we judged this procedure for removal of pore CO_2 with no dissociation of the hydrate (see below) to be a success.

Scanning Electron Microscopy. Images were obtained with a LEO 982 field emission scanning electron microscope equipped with a cryochamber for sample preparation and a cryostage in the microscope (Gatan Alto 2100 cryosystem). Samples were loaded onto a holder then transferred from liquid nitrogen to the preparation chamber at 93 K. A fresh surface free from condensation of atmospheric water was made by fracturing the sample with a scalpel in the preparation chamber, and then this surface was cold sputter-coated with gold−palladium before transferring to the microscope stage. Images were obtained at 2.0 keV and 45 μA, while the sample temperature was maintained between 113 and 123 K.

Powder Diffraction Analysis. Several samples were analyzed by powder X-ray diffraction near 77 K. The diffraction data was collected usually on a middle cross section of the sample cylinder, while liquid nitrogen was dripped onto the sample to maintain low temperature. Samples were scanned from 15° to 48° 2θ at 0.5°/min using Cu Kα radiation (1.5418 Å). Hydrogenous CO_2 hydrate and deuterated CO_2 hydrate were examined by neutron diffraction at the high-resolution powder diffraction beam lines HRPD (Japan Atomic Energy Research Institute, JAERI) and BT-1 (National Institute of Standards and Technology, NIST), respectively. Data from JAERI were collected from 5° to 165° 2θ in 0.05° steps using a monochromatic neutron beam with wavelength 1.163 Å; data were collected between 8 and 215 K at ambient pressures. Data from NIST were collected from 4° to 160° 2θ in 0.05° steps using a monochromatic neutron beam with wavelength 1.540 Å; data were collected at 4.2, 50, 75, and 100 K at ambient pressure. Crystal structure parameters were refined by the Rietveld method using the GSAS software package.[17] More detailed description of the refinement methods are given in Chakoumakos et al.[18] and in a similar study of propane hydrate.[19]

Measurement of CO_2 Gas. Our custom-built, water-based flow meter[20] (see Figure 1) has been used successfully to measure CH_4 gas evolution from dissociating CH_4 hydrate samples.[14,21] To measure CO_2, which is 28 times more soluble than CH_4 in water, several modifications to the apparatus were made: (1) both the water reservoir for the controlled drip system and the flow meter itself were enclosed in CO_2 gas-filled glovebags and the water reservoir was agitated to promote CO_2 dissolution; (2) the gas inlet inside the flow meter cylinder was raised so that the CO_2 gas did not mix the water column as it entered; (3) the flow meter was primed with CO_2 gas several times for a few days prior to the dissociation experiment to promote CO_2 saturation of the water within the cylinder; (4) baseline drifts of 0.1 to 0.3 mV/h in the load-cell output (due to continued solution of CO_2 in the water column during periods of no gas flow) were incorporated into the data analysis. With these modifications, we were able to minimize changes due to CO_2 dissolution during the dissociation measurements. Nonetheless, slow dissolution produced a steady positive baseline drift in the load-cell output data. Because the starting and ending baseline drifts were not equal and the intervening interval was dominated by large changes in load-cell output due to gas flow, there is uncertainty in the baseline correction in this region. We assumed that the baseline drift lies between the starting and ending values, and depending on which baseline correction is applied, we obtained yields of 100% with uncertainties on the order of ±3% in the measurements of hydrate stoichiometry (see below), which are higher than the calculated uncertainty for CH_4 (±1%).[20]

Hydrate Dissociation Experiments. Two types of experiments, both utilized previously to study the dissociation behavior of CH_4 hydrate,[14,22] were performed at 0.1 MPa on CO_2 hydrate: (1) temperature ramping at fixed pressure and (2) pressure release at fixed temperature. In temperature ramping, the CO_2 hydrate sample was first depressurized to conditions in the CO_2 gas stability field (1.0 MPa near 250 K) and then cooled slowly while maintaining P_{CO_2} below the CO_2 liquidus, before equilibrating at 208−210 K at 0.1 MPa for up to 20 min (P, T conditions in the CO_2 hydrate stability field). Then the sample was warmed at an average rate of 13 K/h to 282 K, while both sample and bath temperatures were monitored and while released CO_2 gas was collected in the flow meter. In pressure-release experiments, the CO_2 hydrate sample was equilibrated at some constant temperature between 238 and 277 K, then pressure was lowered to a pressure still in the hydrate and CO_2 gas stability fields. To start the experiment, pressure was rapidly decreased to 0.1 MPa within 20 s, and then internal sample temperature(s) and released CO_2 were monitored continuously, while the external bath temperature was held isothermal. In experiments performed at temperatures below 273 K, the experiments were concluded by warming the samples to 282 K to release the remaining CO_2.

Synthesis and Sample Characterization−Results and Discussion

CO_2 hydrate has been successfully synthesized in bulk from fine-grained seed ice and CO_2 liquid, resulting in complete conversion to hydrate with excess CO_2 liquid remaining. In the two-stage, two-cycle synthesis procedure, the pressure dropped monotonically during the isothermal hold at 267.5 K

(Figure 2a, A1 to A2), as CO_2 reacted with H_2O(s) to form hydrate. The evolution of the CO_2 pressure over time is consistent with the results of Henning et al.[11] on D_2O ice + CO_2 liquid. They determined that about 70% ± 5% of the D_2O converted to CO_2 hydrate after 15 h at 263 K and similar pressures and that the amount of conversion to hydrate after a fixed time interval increased with increasing temperature from 230 to 263 K. Therefore, we surmise that, in our experiments, after 20 h at 267.5 K a significant amount of CO_2 hydrate formation had occurred but that unreacted H_2O still remained.

When the bath was heated to 281 K (Figure 2a, A2 to B1), the internal sample temperature held steady between 270 and 271 K (diamond) as the bath temperature rose continuously and the pressure climbed from 17 to 21 MPa. This thermal buffering does not correspond to any phase boundaries in the CO_2-H_2O system that involve hydrate but parallels the $H_2O(s) = H_2O(l)$ reaction that lies approximately 1.5 K higher at these pressures. We infer that significant melting of the unreacted H_2O occurred (Figure 2a, diamond) and that the melting point was depressed by the solution of CO_2 in H_2O(l). Once the remaining free H_2O(s) melted, temperatures in the sample quickly attained thermal equilibrium with their surroundings. As the samples were held at 281 K (Figure 2a, B1 to B2), the liquid CO_2 pressure continued to drop as the CO_2 hydrate formation reaction proceeded. After 20 h at 281 K, the sample was cooled to ambient freezer temperature (Figure 2a, B2 to C). The temperature and pressure decreased smoothly with time until the temperature neared 265 K, at which point the pressure and the sample temperature abruptly increased because of the freezing of unreacted H_2O(l), which occurs at a depressed temperature in part because of the solution of CO_2 in the H_2O(l).

A second heating cycle over 24 h is required to react the remaining free H_2O (Figure 2b). During heating, the temperatures at the sample top and middle again buffer at 270−271 K for several minutes (diamond), although this thermal signal persists for a shorter time (25 vs 55 min in cycle 1). After another isothermal hold at 281 K for ∼18 h, the samples are cooled to freezer temperature, and no H_2O freezing anomalies appear in the pressure or temperature record. We conclude at this point that the reaction has gone to completion. In an attempt to avoid heating the samples through a second cycle to 281 K, in one experiment the samples were held for >48 h at 281 K during the first two-stage cycle (not shown). When the sample was cooled, the freezing anomaly was much less pronounced in size and duration, but still present, requiring the additional heating cycle for complete conversion to hydrate.

In the single-stage synthesis process for CO_2 hydrate (Figure 2c), the results are similar to those described above for the two-stage, two-cycle process. The buffering between 270 and 271 K (diamond) is again observed and lasts almost an hour. At the isothermal hold temperature of 281 K, the pressure decreases monotonically (Figure 2c, B1 to B2) with an increasingly shallow slope with time (not shown) as hydrate forms. We also observed a distinct overstep of the sample temperature over the external bath temperature by 1−2 K once isothermal conditions were reached at 281 K (Figure 2c, near B1). We believe that this sample temperature increase is due to sufficiently rapid formation of CO_2 hydrate such that heat generated from the exothermic hydrate formation reaction is not exchanged quickly enough with the surroundings to maintain thermal equilibrium. There is no other heat source for raising the vessel temperatures above that of the surrounding bath. Similar temperature oversteps have been observed during the synthesis of larger diameter (3.18 cm) samples of CH_4 hydrate (unpublished data). After 30−50 h at 281 K, no anomalous pressure or temperature increases are observed upon cooling, indicating that complete conversion of H_2O to hydrate with one heating cycle and in less total time (50−70 h versus 85 h) has resulted. Thus, the single-stage procedure initially used for CO_2 hydrate synthesis[2,3] is deemed the more efficient method.

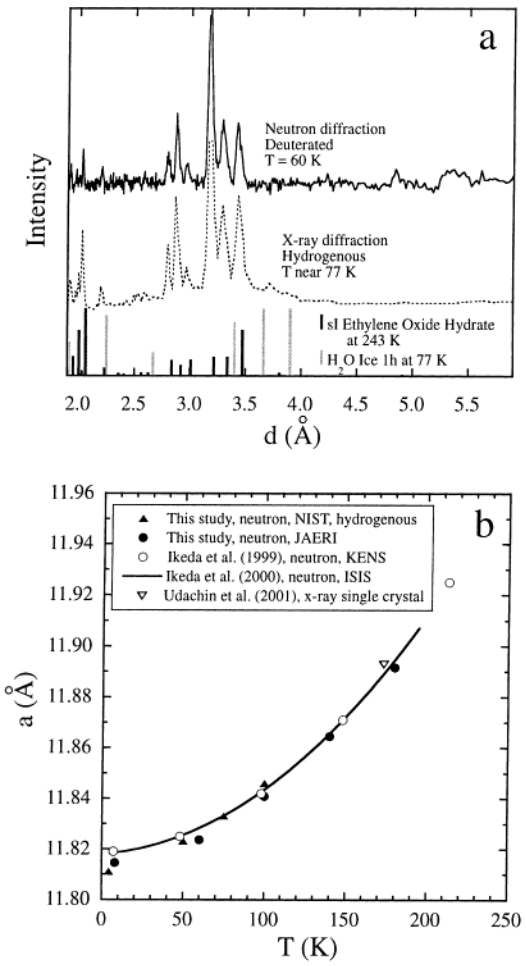

Figure 3. Powder X-ray diffraction pattern (a) of hydrogenous CO_2 hydrate, a portion of the powder neutron diffraction pattern of deuterated CO_2 hydrate, and peak positions and intensities for sI hydrate[23] and H_2O ice. The peak positions obtained for our synthetic CO_2 hydrate samples correspond well to the published positions for sI hydrate (allowing for the systematic offset due to the difference in data collection temperature), although the relative peak intensities do not. The appearance of possible low-intensity ice peaks in the X-ray diffraction patterns of the hydrogenous and deuterated (not shown) CO_2 hydrate samples are not confirmed in the more sensitive neutron diffraction pattern, which probes grain interiors, as well as the surfaces. The likely source of these ice peaks is the unavoidable formation of H_2O ice condensate on the sample surface during data collection. Panel b shows lattice parameter vs temperature for hydrogenous (▲) and deuterated (●) CO_2 hydrate synthesized using our method. Our results are in close agreement with those obtained by Ikeda et al.[10] (○), Udachin et al.[8] (▽), and Ikeda et al.[24] (polynomial fit to data collected between 5 and 195 K at intervals of 10 K) on deuterated samples synthesized at lower pressures.

Samples were characterized in several ways: physical appearance (both macroscopic and by scanning electron microscopy (SEM)), powder X-ray and neutron diffraction analysis, direct measurement of CO_2 uptake by sample weighing, and measurement of the amount of CO_2 released during dissociation. The CO_2 hydrate samples are fine-grained, cohesive, and radially and axially homogeneous. Although the internal thermocouples record a significant H_2O melting event when the samples are

TABLE 1: Rietveld Crystal Structure Refinement Results for CO_2 Deuterate[a]

	T (K)	8	60	100	140	180
	a (Å)	11.8143(7)	11.8241(9)	11.840(1)	11.864(1)	11.891(2)
	ρ_{calc} (g/cm^3)	1.282	1.279	1.274	1.266	1.257
	R_p	0.063	0.062	0.061	0.062	0.061
	χ^2	1.248	1.187	1.145	1.156	1.097
	variables			34		
			Host Atoms			
O_k	x			0		
	y	0.309(1)	0.308(1)	0.306(1)	0.306(2)	0.306(2)
	z	0.119(1)	0.116(1)	0.118(1)	0.114(1)	0.118(2)
	U_{iso} (Å^2)	0.008(1)	0.012(1)	0.015(1)	0.021(3)	0.025(3)
O_i	$x = y = z$	0.1850(9)	0.184(1)	0.187(1)	0.184(1)	0.185(2)
	U_{iso} (Å^2)	0.008(1)	0.012(1)	0.015(1)	0.021(3)	0.025(3)
O_c	x			0		
	y					
	z					
	U_{iso} (Å^2)	0.008(1)	0.012(1)	0.015(1)	0.021(3)	0.025(3)
D_{ik}	x	0.125(2)	0.133(3)	0.118(2)	0.120(3)	0.127(3)
	y	0.226(2)	0.239(3)	0.221(2)	0.227(3)	0.222(3)
	z	0.185(3)	0.184(4)	0.186(3)	0.195(3)	0.188(4)
	U_{iso} (Å^2)	0.040(4)	0.057(6)	0.040(4)	0.041(5)	0.037(5)
D_{ki}	x	0.073(3)	0.078(3)	0.080(2)	0.078(3)	0.074(3)
	y	0.257(2)	0.252(3)	0.264(2)	0.253(3)	0.258(3)
	z	0.142(2)	0.151(3)	0.142(3)	0.140(3)	0.141(3)
	U_{iso} (Å^2)	0.040(4)	0.057(6)	0.040(4)	0.041(5)	0.037(5)
D_{kk}	x			0		
	y	0.314(4)	0.313(4)	0.311(4)	0.319(4)	0.316(5)
	z	−0.041(3)	−0.039(3)	−0.051(3)	−0.045(3)	−0.052(3)
	U_{iso} (Å^2)	0.040(4)	0.057(6)	0.040(4)	0.041(5)	0.037(5)
D_{kc}	x			0		
	y	0.380(4)	0.381(4)	0.366(4)	0.366(4)	0.366(4)
	z	0.130(4)	0.136(4)	0.137(3)	0.142(4)	0.139(4)
	U_{iso} (Å^2)	0.040(4)	0.057(6)	0.040(4)	0.041(5)	0.037(5)
D_{ck}	x			0		
	y	0.428(3)	0.436(4)	0.437(3)	0.440(3)	0.433(4)
	z	0.183(3)	0.172(3)	0.182(3)	0.185(3)	0.185(4)
	U_{iso} (Å^2)	0.040(4)	0.057(6)	0.040(4)	0.041(5)	0.037(5)
D_{ii}	$x = y = z$	0.230(2)	0.232(3)	0.229(2)	0.229(2)	0.231(3)
	U_{iso} (Å^2)	0.040(4)	0.057(6)	0.040(4)	0.041(5)	0.037(5)
			Guest Atoms			
C_S	$x = y = z$	0	0	0	0	0
	U_{iso} (Å^2)	0.014(9)	0.013(8)	0.004(7)	0.02(1)	0.01(1)
O_S	x			−0.0842		
	y			0.0343		
	z			0.0343		
	U_{iso} (Å^2)	0.014(9)	0.013(9)	0.004(7)	0.02(1)	0.01(1)
	n			$^1/_{12}$		
C_L	x			0		
	y					
	z					
	U_{iso} (Å^2)	0.08(1)	0.09(1)	0.06(1)	0.07(1)	0.07(2)
O_{L1}	x			−0.0268		
	y			0.3161		
	z			0.5661		
	U_{iso} (Å^2)	0.08(1)	0.09(1)	0.06(1)	0.07(1)	0.07(2)
	n			$^1/_8$		
O_{L2}	x			0.0268		
	y			0.1839		
	z			0.4339		
	U_{iso} (Å^2)	0.08(1)	0.09(1)	0.06(1)	0.07(1)	0.07(2)
	n			$^1/_8$		

[a] Space group *Pm*3*n*. Atomic site labels follow that of Ikeda et al.,[24] and rigid body constraints are used to describe the guest molecule positions. Occupancies of the deuterium sites were fixed at 0.5. Isotropic displacement parameters for like atoms were constrained to be the same.

warmed through the H_2O ice point (described above), there is no textural evidence that unreacted H_2O coalesced or pooled in the samples. After synthesis is complete, as determined by the absence of anomalous pressure or temperature increases upon cooling through the H_2O ice point, we have pure synthetic CO_2 hydrate that is free of unreacted H_2O (see below). The samples typically contain 37 g of hydrate with a calculated porosity of 44% ± 1%.

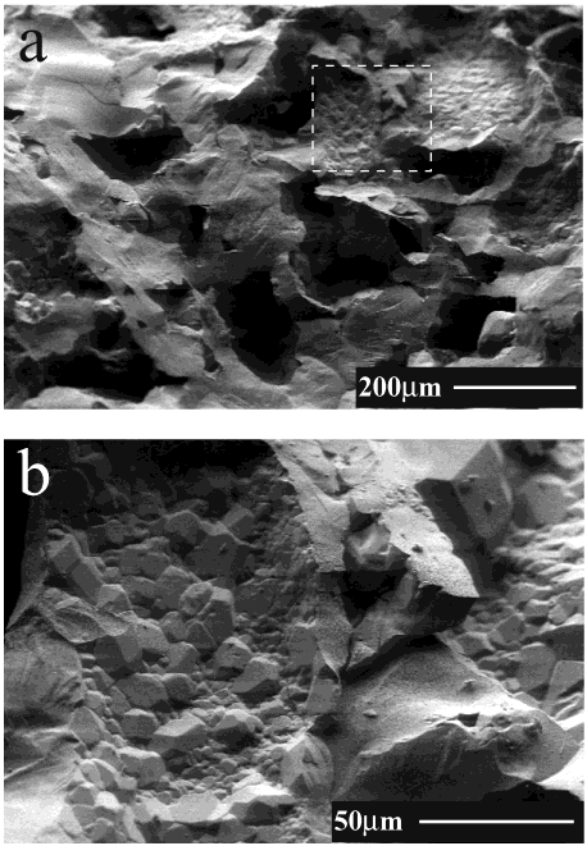

Figure 4. Representative SEM images of deuterated CO_2 hydrate: (a) fractured surface of hydrate, exhibiting densely crystallized regions of CO_2 hydrate with 50−300 μm pore spaces distributed throughout the material. The texture suggests that the original intergranular seed ice porosity persisted during hydrate synthesis but that H_2O mobility on a localized scale has eliminated the original seed ice grain texture. Panel b shows a magnified view (5×) of the area outlined in panel a, showing that the pore cavities are lined with euhedral 1−20 μm grains of hydrate. SEM images of hydrogenous CO_2 hydrate (not shown) exhibit features similar in scale and texture.

X-ray and Neutron Diffraction. The powder X-ray and neutron diffraction patterns of both hydrogenous and deuterated CO_2 hydrate samples exhibit well-defined peaks for sI hydrate and no peaks attributable to solid CO_2 (Figure 3a). The trace ice peaks in X-ray powder patterns of both hydrogenous and deuterated (not shown) CO_2 hydrates were probably due to H_2O condensation from the atmosphere during data collection; no ice was detected by neutron diffraction, confirming that complete conversion of the starting material to deuterate was achieved. Rietveld refinements of the neutron diffraction data yielded thermal expansion for CO_2 hydrate that is consistent with earlier measurements (Figure 3b). Table 1 summarizes the Rietveld structure refinements results for the deuterated CO_2 hydrate. The refinement results are not as precise as those reported by Ikeda et al.;[24] however, we do largely corroborate the temperature-dependent behavior of the mean-square displacements of the guest molecules. One difference in our results is that the isotropic displacements increase in the order host O = CO_2 in small cage < host D < CO_2 in large cage whereas the results of Ikeda et al.[24] are host O < host D < CO_2 in small cage < CO_2 in large cage. The large and nearly temperature-independent displacements of the guest molecules, particularly in the large

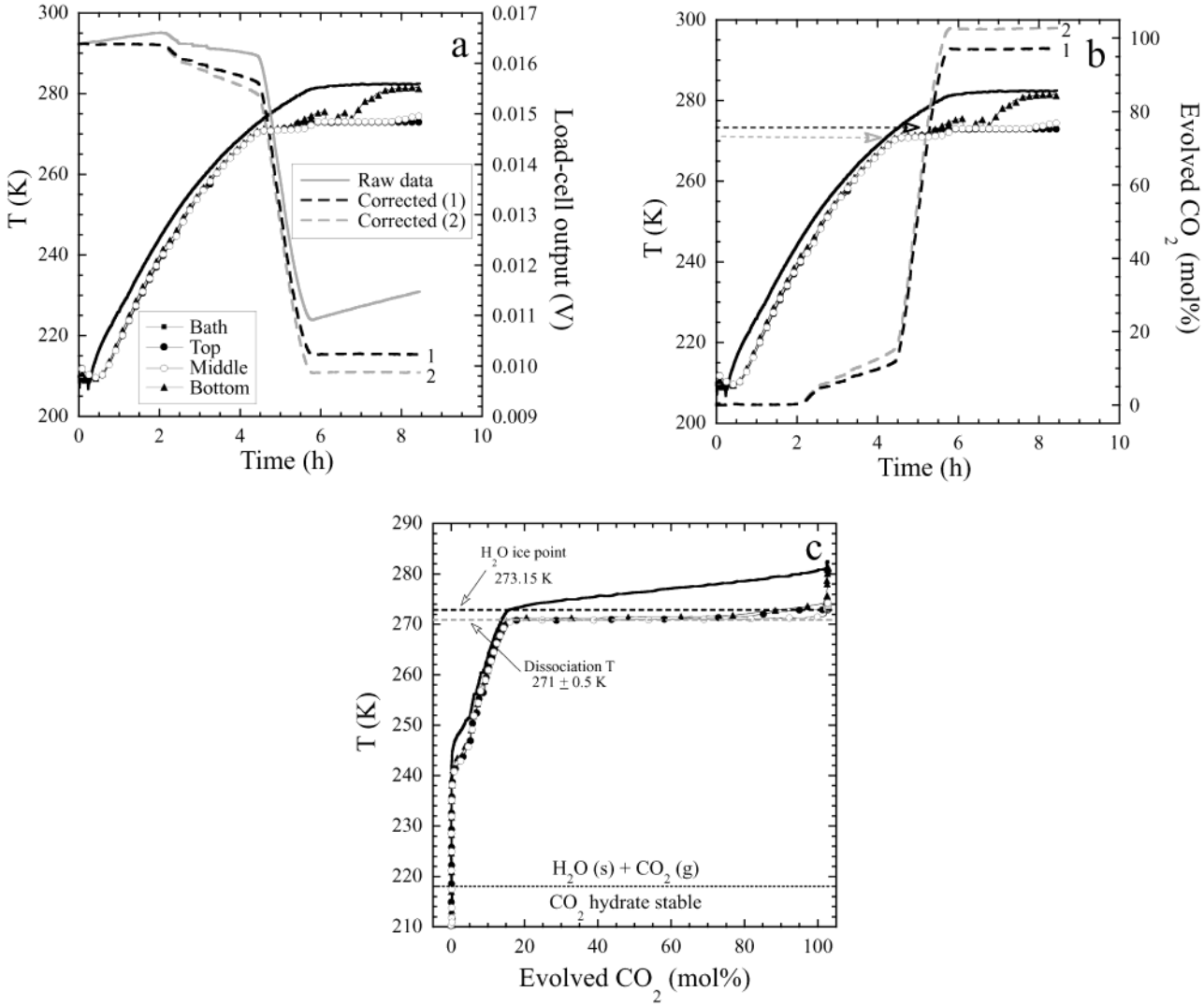

Figure 5. Results from a temperature-ramping experiment at 0.1 MPa on CO_2 hydrate, in which the sample is slowly warmed from 210 to 282 K, resulting in complete dissociation of the hydrate to form H_2O(l and s) and CO_2 gas. In panel a external bath temperature and internal sample temperatures (every tenth data point plotted), as well as the load-cell output from the flow meter (gray line = raw data, gray and black dotted lines = baseline-corrected data), are continuously monitored as the hydrate dissociates and gas is released and collected in the flow meter. The initial baseline drift of the flow meter (0.119 mV/h between 0.5 and 1.8 h) and the final baseline drift (0.257 mV/h between 5.8 and 8.4 h) were collected over the intervals when no gas was evolving from the sample (on the basis of the linearity of the load-cell data and the sample temperature conditions). The baseline-corrected data (curves labeled 1 and 2) represent the range in which the actual corrected load-cell data may fall (see text). Panel b shows the external bath and internal sample temperatures (as in panel a) and the amount of CO_2 gas evolved from the sample during dissociation. Internal sample temperatures are buffered at 271 K for over an hour (gray arrow), during which most of the gas is released from the hydrate, and also at 273 K for several hours (black arrow), during which no gas release occurs (see text for discussion). The buffering at 273 K is less pronounced at the sample bottom where ice melted first and liquid water coalesced. Evolved CO_2 curves 1 and 2 represent the data range after baseline corrections are applied, resulting in an uncertainty of ±3% in the measured total amount of evolved CO_2. Panel c shows the evolution of CO_2 (only curve 2 results shown) vs external bath and internal sample temperatures of CO_2 hydrate (symbols as in panel a). Maximum gas evolution rates of 100 cm^3/min (0.226 mol/h) occur at 271 K.

cage, imply a significant amount of positional disorder about the cage center, that is, movement of the CO_2 molecule off from the cage center position. Earlier diffraction studies yielded stoichiometries for deuterated CO_2 hydrate of 6.20 ± 0.15,[8] 6.1 to 6.7,[11] and 6.3 to 6.9 (depending on synthesis pressures of 6 to 1.5 MPa[9]). It was not possible to extract cage occupancy information from the refinements of the diffraction data; however, we have been able to determine the CO_2 gas contents of the samples by other means (see below).

Mass Uptake Measurements. The mass uptake results are in excellent agreement with the measured gas yields obtained from hydrate dissociation (see below). The mass uptake was measured on two samples that had been flushed with CH_4 gas before quenching in liquid nitrogen. The samples, encased in an indium jacket with a bottom disk used for synthesis, were weighed on a Denver Instruments XP-300 balance (maximum capacity is 300 g with ±0.01 g precision) that is routinely kept in a commercial freezer near 250 K. One sample, synthesized from 25.95 g of seed ice, gained 11.11 g after synthesis, yielding a composition of CO_2·5.71H_2O if all weight gain is attributed to CO_2 occupying hydrate sites. Another sample, synthesized from 25.98 g of seed ice, gained 11.25 g after synthesis, yielding a composition of CO_2·5.64H_2O. Both measurements indicate that the water/carbon dioxide ratio is within 2% of the minimum value of $n = 5.75$ for fully occupied sI hydrate. The systematically high weight gains in part are due to observed H_2O condensation on the indium jacket during weighing; we cannot rule out the possibility that some free CO_2 solidified during the

quenching procedure, although no evidence for solid CO_2 was observed in the diffraction patterns.

SEM Imaging. The CO_2 hydrate samples were imaged using scanning electron microscopy (SEM). A deuterated sample is shown in Figure 4. The dense crystalline hydrate contains large (typically 50−300 μm), irregularly shaped pore structures that are lined with euhedrally faceted hydrate crystals. This porosity is a relic of the starting intergranular seed ice porosity; however, the original ice grain boundaries have been fundamentally altered by hydrate crystallization. We infer a grain size in the hydrate from etching that develops on cleaved surfaces as the sample sits under vacuum in the SEM. This inferred grain size distribution (not shown in Figure 4) is comparable to that of the faceted pore-lining crystals (a few microns to a few tens of microns) and not that of the starting seed ice material (180−250 μm).

Dissociation—Results and Discussion

Dissociation Behavior. The temperature-ramping experiments on CO_2 hydrate yielded consistent results on hydrate gas content and gas release as a function of temperature (Figure 5) but exhibited unexpected dissociation behavior: at most only 20% of the observed CO_2 gas content was released by 270 K, even though phase equilibria data[1] indicate that CO_2 hydrate is stable only below 218 K at 0.1 MPa. The initial gas release occurred between 240 and 250 K in one or two pulses, sometimes sharply defined and accompanied by drops in the sample interior temperature, followed by a slow, steady release between 250 and 270 K. The remaining 80+% of the gas was released above 270 K in a sharply defined event (Figure 5b,c) in which the internal sample temperature was buffered at 271 ± 0.5 K. Once gas evolution ceased, the internal sample temperature climbed to 273.2 K, the melting point of pure H_2O.

Isothermal pressure-release experiments also were performed between 240 and 277 K (Figure 6). In the experiments performed below 273 K, slow, steady CO_2 loss was observed during the isothermal portions of the experiments. Samples released up to 10% of their gas content during the isothermal holds, which lasted 0.3−3.8 h (Figure 6a). The average rate of dissociation (amount of gas released divided by the isothermal hold time) does not correlate simply with increasing temperature (240 K, 10.0 mol %/h; 252 K, 1.2 mol %/h; 268 K, 7.2 mol %/h); however, the facts that the 252 K experiment was on a deuterated sample and that the data set is limited make it impossible to describe the relationship between temperature and dissociation rate in any detail. As samples were heated to 282 K, the observed dissociation behavior was comparable to that observed in the temperature-ramping experiments in that by 270 K (273 K for D_2O sample) up to 20% of the observed CO_2 loss had occurred, although the small, sudden gas releases and accompanying temperature decreases occurred at slightly warmer temperatures (255−265 K). The remaining 80% of the gas was released at 271 ± 0.5 K. In the experiment on the deuterated sample, the buffering temperature of dissociation is displaced +3 K, which is slightly smaller than the difference in melting temperature of D_2O, +3.8 K.

In pressure-release experiments above 273 K (274 and 277 K), dissociation proceeded to completion as the external bath temperature was held isothermal. The internal sample temperatures dropped several degrees following the pressure release. In the 274 K experiment (not shown), the buffering temperature in the sample interior was 271 ± 0.5 K, the same temperature interval observed during dissociation of CO_2 hydrate under nonisothermal conditions (see above). In the 277 K experiment (Figure 6b), the sample interior was depressed below 268 K for more than 50% of the dissociation event and eventually reached 271 K after 75% of the sample dissociated. We suspect that the high rate of dissociation in this experiment may have produced the larger temperature depression.

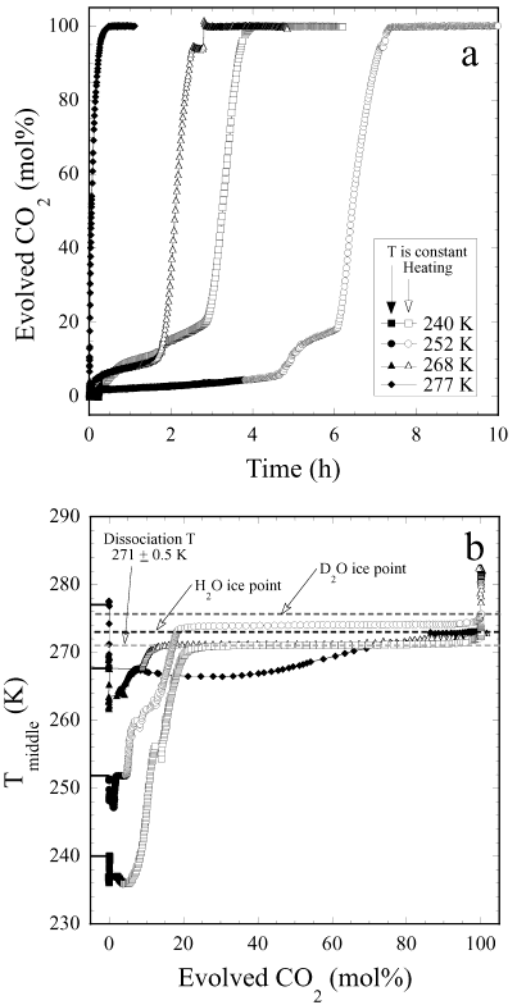

Figure 6. Evolution of CO_2 gas after rapid depressurization of the hydrate sample to 0.1 MPa. A constant external temperature was maintained for some time interval (closed symbols) before heating the sample to 282 K (open symbols); transition from closed to open symbols indicates time at which heating of the external bath began. Temperatures and isothermal hold times are as follows: 240 K, 0.4 h (*T* settled at 238 K for most of isothermal hold); 252 K, 3.8 h (deuterated sample); 268 K, 1.2 h; 277 K, 1.2 h. Panel a shows the evolution of CO_2 from hydrate sample over time. Sample held isothermally at 277 K dissociated completely and did not require further heating. CO_2 gas yields were normalized to 100%; however, actual yields were 90% (240 K), 73% (252 K), 78% (268 K), and 70% (277 K). See text for discussion of low yields. Panel b shows evolution of CO_2 (only curve 2 results shown) vs temperatures of the external bath and sample middle (symbols as in panel a). During the rapid depressurization event, the internal sample temperature drops several degrees due to rapid expansion of the gas but rebounds by the end of the isothermal hold. In experiments performed below 273 K, the sample temperature reequilibrates with the external bath temperature within minutes, while above 273 K sample temperatures remain depressed as rapid dissociation of the hydrate occurs to completion.

Hydrate Stoichiometry. The gas content of the synthetic CO_2 hydrate has been determined from the results of the temperature-ramping experiments, as we did previously for CH_4 hydrate.[20] In three different temperature-ramping experiments, we obtained the following CO_2 yields (with uncertainties of ±3%, as described above): 103%, 102%, and 100%, based on the

TABLE 2: Reported Compositions for Synthetic CO_2 Hydrate

reference	T^a (K)	P_{equil} (MPa)	P^b (MPa)	n	method
Kuhs et al.[9]	273	1.2	1.5−6.0	6.9−6.3	neutron diffraction
Henning et al.[11]	278	2.2	6.2	6.4 ± 0.3	neutron diffraction
Udachin et al.[8]	276	1.7	3.8	6.20 ± 0.15	X-ray diffraction
this study	280	2.8	20.3	5.7	mass uptake
	280	2.8	18.3	5.6	mass uptake
	280.5	3.0	20.1	5.59[c]	dissociation
	280.5	3.0	20.1	5.64[c]	dissociation
	280.5	3.0	17.4	5.74[c]	dissociation

[a] Kuhs et al. and Udachin et al. synthesized hydrate under isothermal conditions, whereas Henning et al. and this study synthesized hydrate at 263−278 K and 250−281 K, respectively. Maximum synthesis temperatures are shown in table. [b] *P* for this study and for Henning et al. is the final pressure reached at the end of synthesis; in this study, initial pressures at 281 K were slightly higher (by up to 3 MPa) and decreased as synthesis reached completion. [c] Uncertainty of ±3 mol % corresponds to an uncertainty in *n* of ±0.15 (see text).

assumption of full occupancy of all cages (i.e., $n = 5.75$). The last experiment, which had a slightly lower gas yield, was annealed near 1.0 MPa and 252 K for 6 days before the temperature-ramping experiment because there was some concern that condensed CO_2 liquid was remaining in the sample after dropping pressure below the CO_2 gas/liquid boundary (this was a significant problem in synthetic propane hydrate samples made from propane liquid, unpublished data). The measured gas yields indicate that approximately all cages in the CO_2 hydrate are filled, which is consistent with the measured mass uptake of these samples (see above, Table 2). Unfortunately, we cannot extract cage occupancy information from the refinement of the neutron diffraction data in this study to corroborate this result.

Partial occupancy of small cages and nearly complete occupancy of large cages in CO_2 hydrate has been determined for previous synthetic CO_2 hydrate samples, which had values of *n* of 6.2 or higher (Table 2). These samples were synthesized at maximum temperatures between 273 and 278 K and at pressures up to 6.0 MPa. In this study, using the methods described above, measured gas contents of CO_2 hydrate have values of *n* near 5.75, suggesting that both small and large cages are approximately filled. Two independent techniques have yielded a consistent hydrate number for samples made under our synthesis conditions, although we acknowledge that the techniques that we have utilized to determine *n* do have significant uncertainties. Kuhs et al.[9] have shown that higher synthesis pressures yield higher cage occupancies ($n = 6.9$ at 1.5 MPa and $n = 6.3$ at 6.0 MPa, both at 273 K), while Udachin et al.[8] suggest that the overstep of the synthesis pressure above the hydrate equilibrium pressure (expressed as a ratio P/P_o) is a relative indicator of the resulting cage occupancies. Since the samples in this study were synthesized at much higher CO_2 liquid pressures (P/P_o of 6−7) than those in the earlier studies (P/P_o between 1 and 5), it is plausible that all cages could be approximately filled.

Comparison with Structure I CH_4 Hydrate

Synthesis. Using the technique developed by Stern et al.,[16] complete conversion of the starting seed ice to sI hydrate is achieved at CH_4 gas or CO_2 gas/liquid pressures well above the equilibrium hydrate phase boundaries and at a range of temperatures that span the H_2O solid/liquid-phase boundary (Figure 7a). The maximum synthesis temperature for CO_2 hydrate is about 10 K lower than that for CH_4 hydrate because

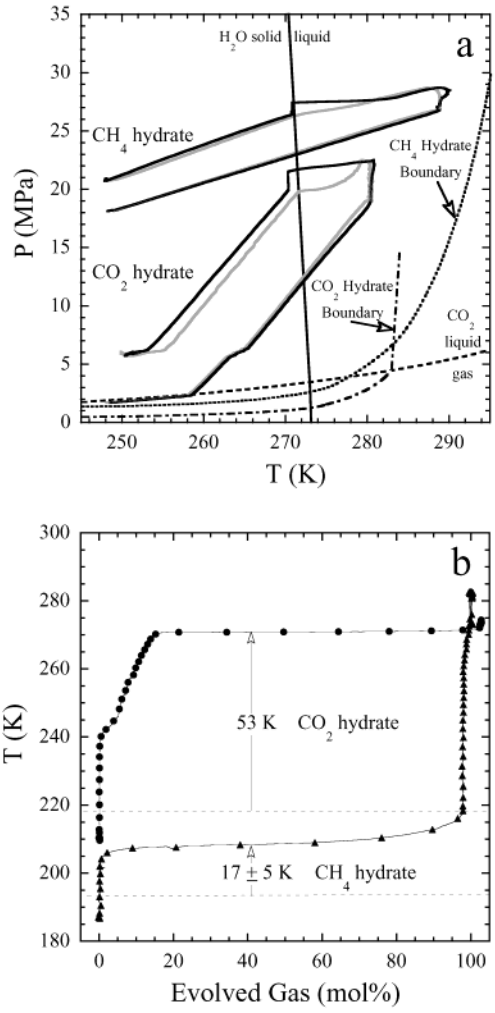

Figure 7. Comparison of sI CO_2 and CH_4 hydrate synthesis and dissociation, illustrating the relationship to their respective hydrate stability boundaries. Panel a shows typical pressure−temperature pathways for CO_2 and CH_4 hydrate synthesis. Bath temperatures (gray curves) and internal sample temperatures (black curves; only the temperature measured at the sample middle is shown, see text) are plotted. Pressure is for either CH_4 gas or CO_2 gas/liquid (see Figure 2). The following phase boundaries are indicated: CH_4 hydrate = CH_4(g) + H_2O(l or s) (•••); CO_2 hydrate = CO_2(g or l) + H_2O(l or s) (−•−); CO_2 g = l (− − −); H_2O s = l (—). The single-stage, single-cycle curve is shown for CO_2 hydrate synthesis. Note that the temperature range over which the CO_2 hydrate sample temperature lags the external bath temperature (near 270 K) is displaced more than a degree below that in the CH_4 hydrate system (see text). Panel b shows the dissociation of CO_2 and CH_4 hydrate in temperature-ramping experiments. Samples were equilibrated at a starting temperature approximately 8 K below the equilibrium hydrate boundary at 0.1 MPa (− − −) and then heated isobarically at a rate of ∼13 K/h. Internal sample temperatures (at sample middle) are shown, and every tenth data point is plotted (data collected at 60 s intervals). Vertical arrows indicate temperature offset between the equilibrium boundary and the dissociation temperature under dynamic heating conditions.

of the steepness of the hydrate phase boundary above the CO_2 liquidus, and the range of CO_2 pressure is controlled by the initial bottle pressure of the CO_2 source. Upon pressurization with hydrate-forming gas (either CH_4 or CO_2) at temperatures below the H_2O melting point, the ice surface converts to hydrate at an observable rate.[2,3] Hydrate growth proceeds at a rate that decreases with time after an initial period of rapid nucleation and growth.[1,25] From their isothermal neutron diffraction experiments below the D_2O ice point, Henning et al.[11] and Wang et al.[26] showed that the rate of conversion increased with increasing

TABLE 3: Comparison of Dissociation Behaviors of CO_2 and CH_4 Hydrates at 0.1 MPa[a]

temperature interval	CO_2 hydrate	CH_4 hydrate
T_{eq} at 0.1 MPa	218 K	193 K
	Temperature-Ramping (from Below T_{eq} to 282 K)	
T_{eq} to T_{eq} + 25 K	<10% of CO_2 is released	≥95% of CH_4 is released
T_{eq} + 25 K to 270 K	>80% of the CO_2 remains	<3% of the CH_4 remains
near $T_{melting}$ of H_2O	remaining gas released (271.0 ± 0.5 K)	remaining gas released (272.5 ± 0.6 K)
	Rapid Depressurization (Experiments at Various T)	
$T_{isothermal} \leq T_{eq}$ + 46 K	<20% of CO_2 is released[b]	≥90% of CH_4 is released[c]
$T_{isothermal}$ = 242−271 K		anomalous preservation[d]
$T_{isothermal}$ to 282 K	remaining gas released (271.0 ± 0.5 K)	remaining gas released (272.5 ± 0.6 K)
$T_{isothermal} \geq$ 273 K	gas released while T buffered at 271.0 ± 0.5 K	gas released while T buffered at 272.5 ± 0.6 K

[a] Note that in all temperature-ramping experiments samples were heated at approximately 13 K/h (see Figures 5 and 7b). In rapid depressurization experiments at $T_{isothermal} \leq T_{eq}$ + 46 K and at $T_{isothermal} \geq$ 273 K, the isothermal portions of the experiments were performed over similar time intervals of up to a few hours (see Figure 6, refs 14 and 21). [b] Isothermal temperatures for individual experiments were 240, 252, and 268 K (268 K is actually +50 K above T_{eq}). [c] Isothermal temperatures ranged from 204 to 239 K at approximately 5 K intervals.[14] [d] Dissociation rates are dramatically depressed relative to measured rates at isothermal temperatures below 239 K and above 272 K. For example, the average rate at 268 K (based on the time required to lose 50% of the sample's gas content) is less than 10^{-4}%/s, whereas at 239 K the rate is 0.8%/s, a difference of 4 orders of magnitude. The rates in this temperature interval vary nonsystematically with increasing temperature.[14]

temperature, which was successfully modeled wherein the rate of reaction depends on a diffusion constant, the ice grain size (assuming spherical grain shapes with a controlled grain size distribution), and determination of the point at which the hydrate growth becomes dominated by diffusion of CO_2 and CH_4 through the external hydrate layer to the unreacted free water core. In an in situ X-ray diffraction study of CO_2 hydrate growth, Takeya et al.[7] also conclude that CO_2 diffusion is the rate-limiting step in hydrate growth below the H_2O melting point.

Complete conversion of the free H_2O to CH_4 or CO_2 hydrate occurs on an efficient time scale of a few days only when the temperature is increased above the H_2O solidus and held at high temperature near the hydrate stability boundary for several hours.[11,16,26] As the temperature nears 273 K, the internal sample temperature is buffered at nearly constant temperature for as much as 1 h while the bath temperature continues to increase at a constant rate, and the buffering temperature decreases slightly as pressure increases (Figure 7a). In the CH_4 system, the buffering temperature is slightly depressed (~0.3 K) below that of the H_2O solidus, while the depression is 1.2 K in the CO_2 system. We attribute the observed thermal buffering to the melting of ice (H_2O or D_2O, as described above), the temperature offsets from the pure H_2O phase boundary to freezing-point depression due to the solubility of CH_4 or CO_2 in the liquid water phase, and the greater offset in the CO_2 system to the greater solubility of CO_2 in water.

The formation of a free water phase during hydrate synthesis can alter the sample texture and obscure the individual ice grain morphology under certain conditions. In optical cell experiments, Stern et al.[2,3] observed that particle morphology of individual grains of loosely packed ice starting material can be maintained as hydrate growth proceeds from the surface inward at temperatures that spanned the H_2O melting point (under optimum synthesis conditions of high pressure above 25 MPa from fine-grained seed ice of ≤250 μm; in experiments that did not meet these conditions, a discrete melt phase was observed). Moudrakovski et al.[27] also showed that, when hydrate-encapsulated ice (100−200 μm) was warmed above the H_2O ice point under moderate CH_4 pressures (6−12 MPa), liquid water formed and remained discretely contained within the hydrate shells. In contrast, SEM micrographs of CO_2 hydrate (Figure 4) and CH_4 hydrates[22] clearly show that a substantial change in texture does occur during hydrate growth in the bulk samples that start with an intergranular ice porosity of nominally 40−50%. The discrete ice grain morphology is no longer evident, and the hydrate crystallizes on a finer scale (typically grains are less than 10−20 μm across) than the starting ice material (200 μm), although some intergranular porosity persists. The observed textures indicate that free H_2O is locally mobile and not confined to the interiors of hydrate-bounded grains, and this may explain the rapid and complete conversion of remaining free H_2O to hydrate at temperatures above the H_2O solidus. These observed textural changes in the closely packed samples suggest that models of inward-diffusion of CO_2 or CH_4 through the outer hydrate layer of a spherical grain may be incomplete for describing nonisothermal hydrate growth at temperatures that span the H_2O ice point. The grain−grain contacts in closely packed ice starting material may spoil the spherical symmetry of the reaction by limiting appreciable gas diffusion at these points of contact.

Dissociation. The dissociation behavior of CO_2 hydrate is in marked contrast to the behavior of hydrocarbon gas hydrates. First, in temperature-ramping experiments at least 80% of the CO_2 hydrate persisted for several hours at temperatures reaching more than 50 K above its equilibrium phase boundary, while sI CH_4 hydrate[14] (Figure 7b, Table 3), sII methane−ethane hydrate,[22] and sII propane hydrate (unpublished data) released >95% of their gas contents within 25 K of their equilibrium boundaries. Second, although the CO_2 hydrate data set is limited, there is no evidence for the complex temperature-dependent dissociation behavior observed in pressure-release experiments on CH_4 hydrate.[14,22] The dissociation rate of CH_4 hydrate increases with increasing temperature up to 239 K (+46 K above T_{eq}, the equilibrium temperature at 0.1 MPa), is significantly depressed between 242 and 272 K (+49 to 79 K above T_{eq}), and then increases with increasing temperature above 272 K (see Table 3). The slowest rates are observed at 268 K (T_{eq} + 75 K). Conversely, the dissociation rate of CO_2 hydrate does not vary considerably with temperature between T_{eq} and 268 K (+50 K). For example, in comparing experiments at +21 K above T_{eq}, CH_4 hydrate released 97% of its gas content in 1.3 h, whereas CO_2 hydrate released less than 10% of its gas content in 0.5 h (or, extrapolating the data, at most 16% in 1.3 h). Third, the pressure-release experiments on CO_2 hydrate at temperatures below 273 K are wholly consistent with the dissociation behavior observed in the temperature-ramping experiments. Again this is in contrast to the behavior of CH_4 hydrate, in which amounts and rates of dissociation in both types of experiments are consistent below 240 K but not between 242 and 272 K. Furthermore, our observations are entirely consistent with the ability of Henning et al.[11] to vent the excess

CO_2 at 263 K and repressurize with a different gas (in their case, He) without appreciable CO_2 hydrate dissociation.

However, in pressure-release experiments above 273 K, the observed dissociation behavior of CO_2 hydrate is similar to that observed for CH_4 hydrate[21] in that regardless of the starting temperature the internal sample temperatures plunge below the H_2O melting point following the pressure release and are buffered in a distinct temperature interval (272.5 ± 0.5 K for CH_4 hydrate) until dissociation nears completion and then climb to the H_2O melting point (Table 3). In the 277 K experiments, we note that in the CO_2 system (1) the temperature depression due to adiabatic cooling from rapid release of gas pressure and the onset of hydrate dissociation is more pronounced (265 vs 271 K) and (2) the time to complete dissociation is less (0.5 vs 1.5 h for CH_4).

In summary, the dissociation behavior of sI CO_2 hydrate is governed by one dominant characteristic: regardless of the pressure−temperature pathway the sample follows to conditions outside the hydrate stability field (i.e., by increasing temperature or by decreasing pressure), on a time scale of at least several hours the bulk of hydrate can persist metastably at 0.1 MPa until the temperature reaches 271 K, at which point all of the remaining CO_2 gas is released. This is in marked contrast to the highly temperature- and path-dependent behavior exhibited by sI CH_4 hydrate below 273 K. However, as temperatures near the H_2O melting point, all of the remaining gas is released from the hydrate, regardless of the identity of the hydrate-forming gas, and the dissociation occurs in well-defined temperature intervals. In pressure-release experiments above 273 K, the dissociation behavior of CO_2 hydrate is closely comparable to that of CH_4 hydrate.

Conclusion

Applying the technique of Stern et al.[16] for making CH_4 hydrate, we have synthesized bulk samples of CO_2 hydrate from H_2O or D_2O ice/liquid and CO_2 liquid. Using a variety of techniques, we characterized the material's composition, microstructure, crystal structure, and dissociation behavior following various *P*, *T* pathways. CO_2 hydrate persists metastably at 0.1 MPa until temperatures near the H_2O solid/liquid phase boundary are reached. This may suggest that for CO_2 hydrate the dissociation to gas + ice is impeded and the formation of liquid water is the key to permitting rapid and complete breakdown of the hydrate. This phenomenon is not unique to CO_2 hydrate in that the final gas release from partially to almost completely dissociated CH_4 hydrate samples also occurs at temperatures just below the H_2O ice point. However, the similarity ends there because the dissociation behavior of hydrate at temperatures below 273 K is as varied as the gas guest molecules themselves.

Acknowledgment. We thank Marina Chiarappa-Zucca of LLNL for analyzing the composition of CH_4-stored CO_2 hydrate samples and B. Hemingway, W. Waite, and two anonymous referees for helpful reviews of the manuscript. This work was performed under the auspices of the U.S. Department of Energy by the Lawrence Livermore National Laboratory under Contract W-7405-ENG-48. It was supported in part by the Natural Gas Hydrate Program of U.S. Department of Energy, National Energy and Technology Laboratory, and the Laboratory Directed Research and Development Programs of Oak Ridge National Laboratory (ORNL). We also acknowledge the support of the Japan Atomic Energy Research Institute and the National Institute of Science and Technology, U.S. Department of Commerce, for providing the neutron research facilities used in this work. ORNL is managed by UT-Battelle, LLC for the U.S. Department of Energy under Contract No. DE-AC05-00OR22725.

References and Notes

(1) Sloan, E. D. *Clathrate Hydrates of Natural Gases*, 2nd ed; Marcel Dekker: New York, 1998.

(2) Stern, L. A.; Hogenboom, D. L.; Durham, W. B.; Kirby, S. H.; Chou, I.-M. *J. Phys. Chem. B* **1998**, *102*, 2627.

(3) Stern, L. A.; Kirby, S. H.; Durham, W. B. *Energy Fuels* **1998**, *12*, 201.

(4) Ratcliffe, C. I.; Ripmeester, J. A. *J. Phys. Chem.* **1986**, *90*, 1259.

(5) Ripmeester, J. A.; Ratcliffe, C. I. *Energy Fuels* **1998**, *12*, 197.

(6) Fleyfel, F.; Devlin, J. P. *J. Phys. Chem.* **1988**, *92*, 631.

(7) Takeya, S.; Hondoh, T.; Uchida, T. In *Gas Hydrates: Challenges for the Future*; Holder, G., Bishnoi, P., Eds.; New York Academy of Sciences: New York, 2000; pp 973−982.

(8) Udachin, K. A.; Ratcliffe, C. I.; Ripmeester, J. A. *J. Phys. Chem. B* **2001**, *105*, 4200.

(9) Kuhs, W. F.; Chazallon, B.; Klapproth, A.; Pauer, F. *Rev. High-Pressure Sci. Technol.* **1998**, *7*, 1147.

(10) Ikeda, T.; Yamamuro, O.; Matsuo, T.; Mori, K.; Torii, S.; Kamiyama, T.; Izumi, F.; Ikeda, S.; Mae, S. *J. Phys. Chem. Solids* **1999**, *60*, 1527.

(11) Henning, R. W.; Schultz, A. J.; Thieu, V.; Halpern, Y. *J. Phys. Chem. A* **2000**, *104*, 5066.

(12) Aya, I.; Yamane, K.; Nariai, H. *Energy* **1997**, *22*, 263.

(13) Brewer, P. G.; Friederich, G.; Peltzer, E. T.; Orr, F. M. *Science* **1999**, *284*, 943.

(14) Stern, L. A.; Circone, S.; Kirby, S. H.; Durham, W. B. *J. Phys. Chem. B* **2001**, *105*, 1756.

(15) Rehder, G.; Kirby, S. H.; Durham, W. B.; Brewer, P. G.; Stern, L. A.; Peltzer, E. T. *Geochim. Cosmochim. Acta*, submitted for publication, Fall 2002.

(16) Stern, L. A.; Kirby, S. H.; Durham, W. B. *Science* **1996**, *273*, 1843.

(17) Larson, A. C.; Von Dreele, R. B. *General Structure Analysis System*; Report LAUR 86-748; Los Alamos National Laboratory: Los Alamos, NM, 1994.

(18) Chakoumakos, B. C.; Rawn, C. J.; Rondinone, A. J.; Marshall, S. L.; Stern, L. A.; Circone, S.; Kirby, S. H.; Jones, C. Y.; Toby, B. H.; Ishii, Y. *Proceedings of the Fourth International Conference on Gas Hydrates*, Yokohama, Japan; 2002; Vol. 2, pp 655−658.

(19) Rawn, C. J.; Rondinone, A. J.; Chakoumakos, B. C.; Circone, S.; Stern, L. A.; Kirby, S. H.; Ishii, Y. *Can. J. Phys.*, **2003**, *81*, 431.

(20) Circone, S.; Kirby, S. H.; Pinkston, J. C.; Stern, L. A. *Rev. Sci. Instrum.* **2001**, *72*, 2709.

(21) Circone, S.; Stern, L. A.; Kirby, S. H.; Pinkston, J. C.; Durham, W. B. In *Gas Hydrates: Challenges for the Future*; Holder, G., Bishnoi, P., Eds.; New York Academy of Sciences: New York, 2000; pp 544−555.

(22) Stern, L. A.; Circone, S.; Kirby, S. H.; Durham, W. B. *Can. J. Phys.* **2003**, *81*, 271.

(23) McMullan, R. K.; Jeffrey, G. A. *J. Chem. Phys.* **1965**, *42*, 2725.

(24) Ikeda, T.; Mae, S.; Yamamuro, O.; Matsuo, T.; Ikeda, S.; Ibberson, R. M. *J. Phys. Chem. A* **2000**, *104*, 10623.

(25) Hwang, M. J.; Wright, D. A.; Kapur, A.; Holder, G. D. *J. Inclusion Phenom. Mol. Recognit. Chem.* **1990**, *8*, 103.

(26) Wang, X.; Schultz, A. J.; Halpern, Y. *J. Phys. Chem. A* **2002**, *106*, 7304.

(27) Moudrakovski, I. L.; Ratcliffe, C. I.; McLaurin, G. E.; Simard, B.; Ripmeester, J. A. *J. Phys. Chem. A* **1999**, *103*, 4969.